Energy and centrality dependence of deuteron and proton production in Pb+Pb collisions at relativistic energies

T. Anticic,[19] B. Baatar,[8] D. Barna,[4] J. Bartke,[6] M. Behler,[13] L. Betev,[9] H. Białkowska,[17] A. Billimeier,[9] C. Blume,[7] B. Boimska,[17] M. Botje,[1] J. Bracinik,[3] R. Bramm,[9] R. Brun,[10] P. Bunčić,[9,10] V. Cerny,[3] P. Christakoglou,[2] O. Chvala,[15] G. E. Cooper,[20] J. G. Cramer,[16] P. Csató,[4] P. Dinkelaker,[9] V. Eckardt,[14] P. Filip,[14] H. G. Fischer,[10] Z. Fodor,[4] P. Foka,[7] P. Freund,[14] V. Friese,[7,13] J. Gál,[4] M. Gaździcki,[9] G. Georgopoulos,[2] E. Gładysz,[6] S. Hegyi,[4] C. Höhne,[13] P. Jacobs,[20] K. Kadija,[19] A. Karev,[14] V. I. Kolesnikov,[8] T. Kollegger,[9] R. Korus,[12] M. Kowalski,[6] I. Kraus,[7] M. Kreps,[3] M. van Leeuwen,[1] P. Lévai,[4] A. I. Malakhov,[8] C. Markert,[7] B. W. Mayes,[11] G. L. Melkumov,[8] C. Meurer,[9] A. Mischke,[7] M. Mitrovski,[9] J. Molnár,[4] St. Mrówczyński,[12] G. Pálla,[4] A. D. Panagiotou,[2] K. Perl,[18] A. Petridis,[2] M. Pikna,[3] L. Pinsky,[11] F. Pühlhofer,[13] J. G. Reid,[16] R. Renfordt,[9] W. Retyk,[18] C. Roland,[5] G. Roland,[5] M. Rybczyński,[12] A. Rybicki,[6,10] A. Sandoval,[7] H. Sann,[7] N. Schmitz,[14] P. Seyboth,[14] F. Siklér,[4] B. Sitar,[3] E. Skrzypczak,[18] G. Stefanek,[12] R. Stock,[9] H. Ströbele,[9] T. Susa,[19] I. Szentpétery,[4] J. Sziklai,[4] T. A. Trainor,[16] D. Varga,[4] M. Vassiliou,[2] G. I. Veres,[4] G. Vesztergombi,[4] D. Vranić,[7] S. Wenig,[10] A. Wetzler,[9] Z. Włodarczyk,[12] N. Xu,[20] I. K. Yoo,[7,13,*] J. Zaranek,[9] and J. Zimányi[4]

(NA49 Collaboration)

[1]*NIKHEF, Amsterdam, Netherlands*
[2]*Department of Physics, University of Athens, Athens, Greece*
[3]*Comenius University, Bratislava, Slovakia*
[4]*KFKI Research Institute for Particle and Nuclear Physics, Budapest, Hungary*
[5]*MIT, Cambridge, Massachusetts 02139, USA*
[6]*Institute of Nuclear Physics, Cracow, Poland*
[7]*Gesellschaft für Schwerionenforschung (GSI), Darmstadt, Germany*
[8]*Joint Institute for Nuclear Research, Dubna, Russia*
[9]*Fachbereich Physik der Universität, Frankfurt, Germany*
[10]*CERN, Geneva, Switzerland*
[11]*University of Houston, Houston, Texas, USA*
[12]*Institute of Physics Świetokrzyska Academy, Kielce, Poland*
[13]*Fachbereich Physik der Universität, Marburg, Germany*
[14]*Max-Planck-Institut für Physik, Munich, Germany*
[15]*Institute of Particle and Nuclear Physics, Charles University, Prague, Czech Republic*
[16]*Nuclear Physics Laboratory, University of Washington, Seattle, Washington 98195, USA*
[17]*Institute for Nuclear Studies, Warsaw, Poland*
[18]*Institute for Experimental Physics, University of Warsaw, Warsaw, Poland*
[19]*Rudjer Boskovic Institute, Zagreb, Croatia*
[20]*Lawrence Berkeley National Laboratory, Berkeley, California 94720, USA*

(Received 21 August 2003; published 10 February 2004)

The transverse mass m_t distributions for deuterons and protons are measured in Pb+Pb reactions near midrapidity and in the range $0<m_t-m<1.0$ (1.5) GeV/c^2 for minimum bias collisions at 158*A* GeV and for central collisions at 40 and 80 *A* GeV beam energies. The rapidity density dn/dy, inverse slope parameter T and mean transverse mass $\langle m_t\rangle$ derived from m_t distributions as well as the coalescence parameter B_2 are studied as a function of the incident energy and the collision centrality. The deuteron m_t spectra are significantly harder than those of protons, especially in central collisions. The coalescence factor B_2 shows three systematic trends. First, it decreases strongly with increasing centrality reflecting an enlargement of the deuteron coalescence volume in central Pb+Pb collisions. Second, it increases with m_t. Finally, B_2 shows an increase with decreasing incident beam energy even within the SPS energy range. The results are discussed and compared to the predictions of models that include the collective expansion of the source created in Pb+Pb collisions.

DOI: 10.1103/PhysRevC.69.024902 PACS number(s): 25.75.Dw

I. INTRODUCTION

In the study of the evolution of nuclear systems created in relativistic heavy ion collisions [1], emitted nucleons and light nuclei carry important information on dynamics of nuclear interactions. There is evidence that in the early stage of high energy nucleus-nucleus collisions the nuclear matter is highly compressed and hot, reaching energy densities an order of magnitude greater than that of normal nuclear matter [2]. This system (fireball) expands and cools, and the interaction among the particles finally ceases. It is in the latest stage of the evolution of the fireball, called the stage of

*Present address: Department of Physics, Pusan National University, Republic of Korea.

freeze-out, that fragile light nuclei, in particular deuterons, are formed. Due to their small binding energy it is improbable that they survive repeated collisions inside the fireball. They are also unlikely to be the fragments of the projectile or the target because of the violence of heavy ion collisions. Thus, the observed deuterons are believed to be created by coalescence of protons and neutrons at freeze-out.

In general, coalescence models relate the invariant yield of light nuclei with mass A to the Ath power of the proton yield [3], assuming the neutron and proton distributions to be identical:

$$E_A \frac{d^3N_A}{dp_A^3} = B_A \left(E_p \frac{d^3N_p}{dp_p^3} \right)^A, \quad p_A = Ap_p, \tag{1}$$

The coalescence factor B_A, which characterizes the coalescence probability, depends on the fireball size as well as its internal dynamics. It can be measured in the experiment and used for estimating the reaction volume in which the composite particles are created. Several prescriptions were proposed to calculate a source radius from the B_A parameter [4–7]. In these models the coalescence parameter scales with the reaction volume as $B_A \propto (1/V)^{A-1}$.

Originally simple momentum-space coalescence models [8], which assumed coalescence to take place between nucleons with a small momentum difference, successfully described early measurements of light nuclei production in nucleus-nucleus collisions at Bevalac and SIS energies of 0.2–2.0 A GeV [9,10]. Furthermore, the B_2 values obtained for these low energy $A+A$ collisions and for $p+A$ collisions at the CERN SPS and FNAL [11] turned out to be relatively independent of the beam energy and the size of the colliding systems.

However, in heavy ion collisions at the typical AGS energies of 10–14 A GeV [12–16] and at 158A GeV at CERN [17–19] B_A was found to be an order of magnitude smaller. This observation was attributed to the larger source volume due to hydrodynamic expansion of the collision zone before freeze-out, a phenomenon not expected to appear at low energy $A+A$ and high energy $p+A$ collisions mentioned above. Thermal and density matrix coalescence models [5,6] had already been developed which considered a significant expansion of the collision volume, albeit no correlations between position and momentum of the nucleons. The presence of collective motion (flow) leads not only to an expansion of the collision volume but also to significant position-momentum correlations between particles at freeze-out [20–22] affecting the process of cluster formation. Indeed, the overall expansion of the system tends to reduce the coalescence probability B_A by spatially isolating nucleons from each other, whereas the collective flow increases B_A. Radial flow makes it more likely for nucleons close in configuration space to have also similar momenta. Thus cluster formation becomes more probable.

Advanced coalescence models [23–25] have recently been developed for systems with strong collective expansion and a large source volume. It was found that the inverse slope systematics of proton and deuteron inclusive transverse mass spectra, and the dependence of B_A on the transverse momentum both arise from an interplay of transverse flow and the radial dependence of the nucleon density. In this context, an experimental study of the production of light nuclei at different beam energies and collision centralities is of great importance since it may help to disentangle the competing effects governing nuclear cluster formation.

New measurements of proton and deuteron production, both in centrality selected Pb+Pb collisions at top SPS energy, 158A GeV, and in central Pb+Pb collisions at 80 and 40 A GeV are presented in this paper.

II. EXPERIMENTAL METHOD

The experiment was carried out with the NA49 large acceptance hadron detector [26] using external ^{208}Pb ion beams with energies of 40, 80, and 158 GeV per nucleon produced by the CERN SPS. Charged particles emitted from collisions in a Pb target of 224 mg/cm^2 thickness (equivalent to 0.47% interaction length) are detected over a large fraction of phase space by tracking in four large volume time projection chambers (TPCs). Two of them (vertex TPCs) are located inside the magnetic field, the two others (main TPCs) are placed downstream of the magnets on either side of the beam line. Particle momentum and velocity are determined from tracking through the magnetic field and measuring the specific energy loss dE/dx in the TPC gas with a resolution of about 4%. Two 2.2-m^2 time-of-flight (TOF) walls containing 891 scintillator pixels each are situated symmetrically behind the main TPCs on both sides of the beam. The average overall time resolution of these detectors is 60–70 ps. In this analysis, the identification of protons and deuterons was primarily accomplished by the TOF measurement, the dE/dx information from the large TPCs being employed to eliminate the background of charged pions and kaons. To demonstrate the TOF identification capability, a sample of the mass spectra obtained from measured momenta and time of flight are shown in Fig. 1.

Online event characterization and triggering is accomplished by beam definition detectors located in the beam line upstream of the target and interaction counters and calorimeters downstream of the target. The data samples were recorded with two trigger settings, providing the selection of central and minimum bias events.

For central Pb+Pb collisions, the primary trigger detector is a zero degree calorimeter (ZDC) located downstream of the detector behind a collimator, which measures the energy E_{ZDC} of the remaining projectile fragments and spectator protons and neutrons. The upper limit on the energy in the ZDC was set to accept the 12% most central events at 158A GeV and 7% at 40 and 80 A GeV from all inelastic Pb+Pb collisions.

For the selection of minimum bias Pb+Pb collisions, a Cherenkov counter in the gas region immediately behind the target is used to veto noninteracting projectiles. Triggering is accomplished by placing an upper threshold on the signal from this Cherenkov counter in coincidence with a valid signal from the beam detectors. Additionally, offline cuts were made on the z position of the fitted primary vertex along the beam direction to minimize the fraction of nontarget background events.

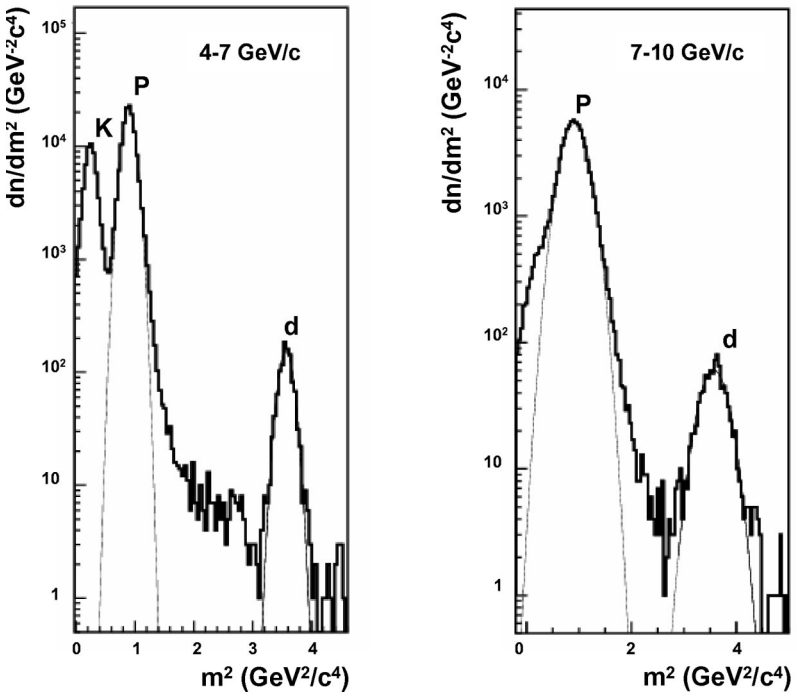

FIG. 1. Mass squared distributions for particles in the momentum ranges $p=4-7$ GeV/c (left) and $p=7-10$ GeV/c (right). Gaussian fit to the proton and deuteron mass peaks is indicated by dashed lines.

III. DATA ANALYSIS AND RESULTS

For the present study of 158*A* GeV Pb+Pb collisions 320 000 central and 735 000 minimum bias events were used. Centrality samples of Pb+Pb collisions were selected subdividing the range of energy E_{ZDC} measured in the ZDC into six bins. In each centrality bin, a direct estimate of the number of participating nucleons N_{part} is made by calculating the net baryon number carried by all particles emitted from the collision into the phase space region outside the spectator region [27]. For this calculation, the charged particle spectra measured in the NA49 experiment for almost the full forward hemisphere [27–29] were used with only a small extrapolation out to the beam rapidity. VENUS [30] and RQMD [31] event generators were employed to relate $\langle N_{part}\rangle$ to the range of the impact parameter b.

In a second approach, an estimate of the number of spectators in an event via a direct measurement of the energy deposited in the ZDC by projectile spectators was used. This method relies on both the event generator and a GEANT simulation of the calorimeter response. The above estimates of N_{part} from the measured final spectra and the energy in the ZDC agree well. The mean value from these estimates was used for $\langle N_{part}\rangle$, and their spread was considered to estimate the systematic uncertainty. They are shown in Table I representing numerical values of centrality parameters used in the analysis. The estimate of the impact parameter b is also based on the E_{ZDC} measurement through the correlation of b with the energy in the ZDC in the simulation. In addition, the number of wounded nucleons $\langle N_W\rangle$ was obtained from a Glauber calculation using the spectator-participant model of nucleus-nucleus collisions.

The data analysis procedure included the following steps. Tracks reconstructed in the TPCs having momentum and dE/dx information were extrapolated to the TOF detector wall and assigned a mass squared value m^2 derived from the momentum and the time-of-flight measurement. Further, only those tracks were accepted for analysis which had a single hit in a scintillator pixel of the TOF detector, i.e., double hits and conversion pairs from γs in the scintillator were rejected, and relevant inefficiency corrections have been applied to the particle yields. The sum of the losses as determined experimentally from the TPC tracking data (double hit) and the charge measurements in the TOF (γ conversion) amounts to 25% on average, with a maximum of 30% in the region of the TOF wall closest to the beam.

Tracks were then subjected to identification cuts applied to the dE/dx and m^2 values in order to select deuterons or protons and to reject pions and most of the kaons. These cuts were chosen in order to optimize the rate of deuterons (protons) and to minimize the background contribution stemming mostly from the other charged particles. Correction factors

TABLE I. Pb+Pb centrality bins from most central (1) to peripheral (6). Columns show the E_{ZDC}/E_{beam} range, the covered range in fraction of the total cross section σ_{tot}, the mean numbers of participating $\langle N_{part}\rangle$ and wounded $\langle N_W\rangle$ nucleons for each bin, and the range of the impact parameter b for the corresponding cross sections.

Bin	E_{ZDC}/E_{beam}	Fraction of σ_{tot}(%)	$\langle N_{part}\rangle$	$\langle N_W\rangle$	b range (fm)
1	0–0.25	0–5	366±8	352	0–3.4
2	0.25–0.40	5–12	309±10	281	3.4–5.3
3	0.40–0.58	12–23	242±10	204	5.3–7.4
4	0.58–0.71	23–33	178±10	134	7.4–9.1
5	0.71–0.80	33–43	132±10	88	9.1–10.2
6	0.80–1.00	43–100	85±6	42	10.2–14.0

for deuteron (proton) loss and residual background contamination due to the cuts were estimated from the experimental dE/dx and m^2 distributions using their parametrized description obtained from the fit. The background and particle losses were negligible in the momentum range up to $p = 5.0$ GeV/c reaching about 20% at highest momenta of $p = 10.0-12.0$ GeV/c.

The identified protons are contaminated by protons from weak decays of strange baryons (feed-down protons) that were incorrectly reconstructed as tracks from the primary vertex. They were subtracted from the proton spectra in order to obtain the true proton distribution at freeze-out. This background correction was obtained from a GEANT-based Monte Carlo simulation of the decay of Λ and Σ hyperons and reconstruction of their charged decay products. For generating representative phase space distributions of the decaying hyperons recent results from the SPS experiments WA97 [32] and NA49 [33] on Λ production including those from Σ^0 decays were used. The small fraction of protons from Σ^+ decays was calculated using the RQMD model simulation.

The overall contribution of feed-down protons was found to be 20–25% and almost independent of the collision centrality. The calculated m_t-spectra of feed-down protons are well described by an exponential function with inverse slope parameter T values gradually changing from 240 MeV to 205 MeV from the most central to the peripheral bins, respectively. Since a large part of the feed-down comes from Λ hyperons, the estimated systematic uncertainty of the feed-down correction is relatively small (5–10 %) and depends only slightly on the collision centrality.

The data were corrected for geometrical acceptance losses using the Monte Carlo simulation of the detector in GEANT. The track reconstruction efficiency was determined by simulation using the method of embedding tracks into real events. The tracking efficiency was found to be nearly 100% in the kinematical range covered by the TOF acceptance.

After all corrections mentioned above, the invariant transverse mass ($m_t = \sqrt{p_t^2 + m^2}$, m–particle mass) spectra for deuterons and protons were obtained (see Fig. 2). The m_t dependence was fitted by the sum of two exponential functions,

$$\frac{d^2n}{m_t dm_t dy} = C_1 e^{-(m_t - m)/T} + C_2 e^{-(m_t - m)/T'}, \qquad (2)$$

the first of them containing the inverse slope T for $m_t - m > 0.2$ GeV/c^2 (to be quoted hereinafter) where no deviation from a single exponential is visible, and the second one describing a deficit from this exponential at low m_t which is estimated to diminish from nearly 10% to almost zero for the most central and peripheral bins, respectively, as compared to the total yield. This expression is found to describe the data well, especially in central interactions where the deviation from the Boltzmann-type distribution is more pronounced.

The numerical values for the inverse slope T and the particle yield dn/dy are given in Table II. The total yield dn/dy was obtained by integrating the transverse mass spectra over the whole m_t range using the fitted function of Eq. (2). The table contains also the values of the mean transverse mass $\langle m_t \rangle - m$. To obtain $\langle m_t \rangle$ averaged over the full kinematical range, an extrapolation to high m_t was made. This extrapolation is typically less than 10% and 20% for protons and deuterons, respectively, and was done by using the fitted function of Eq. (2).

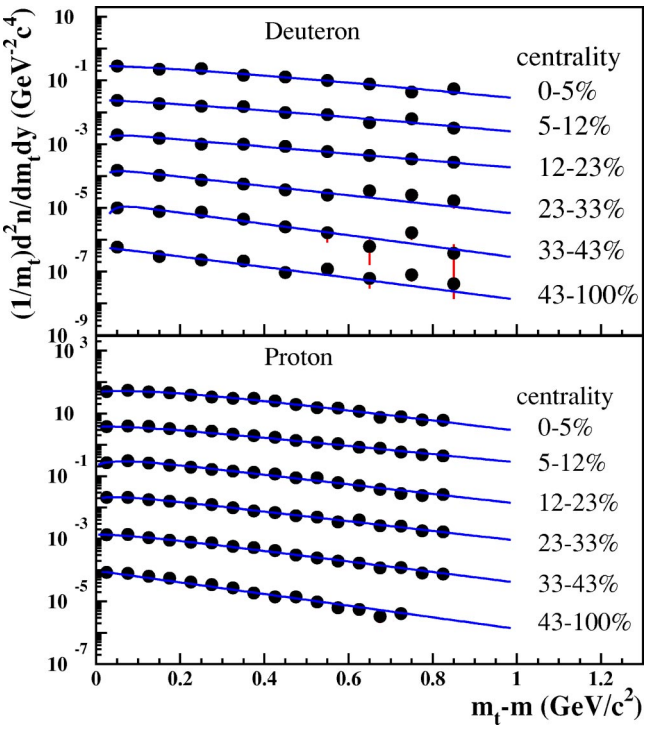

FIG. 2. (Color online) Transverse mass distributions for deuterons in rapidity bin $2.0 < y < 2.5$ and for protons in rapidity bin $2.4 < y < 2.8$ measured at various centralities of 158A GeV Pb+Pb collisions. The curves through the measured points represent fits by Eq. (2). The spectra are scaled down by a factor of 10 successively from the most central data.

TABLE II. Particle yield dn/dy, inverse slope T, and mean transverse mass $\langle m_t \rangle - m$ for deuterons ($2.0 < y < 2.5$) and protons ($2.4 < y < 2.8$) at various centralities in 158A GeV Pb+Pb collisions. The errors are statistical.

Particle	Centrality (% of σ_{tot})	dn/dy	T (MeV)	$\langle m_t \rangle - m$ (MeV/c^2)
Deuteron	0–5	0.33±0.03	425±39	540±50
	5–12	0.27±0.03	421±44	530±48
	12–23	0.21±0.03	416±38	491±45
	23–33	0.12±0.02	330±33	380±38
	33–43	0.08±0.01	279±28	315±32
	43–100	0.04±0.01	279±35	315±39
Proton	0–5	29.6±0.9	308±9	413±13
	5–12	22.2±0.6	308±9	415±14
	12–23	14.5±0.4	276±9	362±12
	23–33	9.8±0.3	273±10	355±12
	33–43	5.7±0.2	245±10	315±13
	43–100	2.9±0.1	216±10	259±12

The sources of considered systematic uncertainties include possible errors in the determination of the efficiency corrections, in particular those for selection of single track hits in the TOF pixels as well as those for particle identification and background subtraction. The subtraction is particularly relevant to the deuterons at the highest momenta and the most peripheral bins which have relatively poor statistics. For protons, an additional systematic error is contributed by the feed-down corrections. The estimate of the particle yield dn/dy represents an extrapolation into unmeasured regions under the explicit assumption of a certain shape of the m_t distribution. For the deuteron results, the systematic errors do not exceed the statistical errors. Resulting total errors for the inverse slope parameters T are 40–50 MeV, almost independent of centrality. For the particle yield dn/dy, they vary from 15% to 30% for central and peripheral bins, respectively. The overall uncertainty of the proton results receives about equal contributions from statistical and systematic errors and is estimated to be $\approx$15 MeV for T. For dn/dy, it slightly increases from 5% to 10% from the most central to the peripheral bins, respectively.

Invariant spectra were also obtained at beam energies of 40 and 80 A GeV for the 7% most central Pb+Pb collisions which corresponds to a mean number of participating nucleons of $\langle N_{part}\rangle = 349$. The data are measured close to midrapidity, namely, in the rapidity range of $1.7 < y < 2.2$ for deuterons and $1.9 < y < 2.3$ for protons at 40A GeV ($y_{\text{c.m.}} = 2.22$), and $1.8 < y < 2.3$ for deuterons and $2.1 < y < 2.5$ for protons at 80A GeV ($y_{\text{c.m.}} = 2.56$).

The number of analyzed events was about 400 000 for 40A GeV and 300 000 for 80A GeV. Analysis of the data was performed in the same manner as for 158A GeV. For the proton feed-down correction, the NA49 results [33] on Λ production at 40 and 80 A GeV obtained from the same data sample were used.

Figure 3 depicts the deuteron and proton spectra for all three energies together with fits by the double exponential function Eq. (2). Again, an obvious deviation from a single exponential shape is seen. The numerical values of the particle yield dn/dy, inverse slope T, and the mean transverse mass $\langle m_t\rangle - m$ are listed in Table III.

IV. DISCUSSION

The transverse mass spectra for deuterons in Pb+Pb collisions at 158A GeV are observed to be significantly harder than those for protons, especially in central collisions. This is illustrated in Fig. 4 where the average transverse mass $\langle m_t\rangle - m$ is plotted as a function of the number of participating nucleons N_{part}. For all centralities, $\langle m_t\rangle - m$ is larger for deuterons and this effect is most pronounced in central collisions. It is also seen that the mean transverse mass of deuterons and protons decreases with diminishing centrality converging approximately to a single value of $\langle m_t\rangle - m \simeq 200$–$250$ MeV/c^2 in the most peripheral interactions. A similar trend with the collision centrality is observed for inverse slopes.

From central data at 40, 80, and 158 A GeV, there is clear evidence that the m_t spectra for both deuterons and protons get flatter with increasing incident energy. An obvious deviation from a single exponential at small m_t, the so called "shoulder-arm shape" of the transverse mass distributions [34], is observed for all three energies.

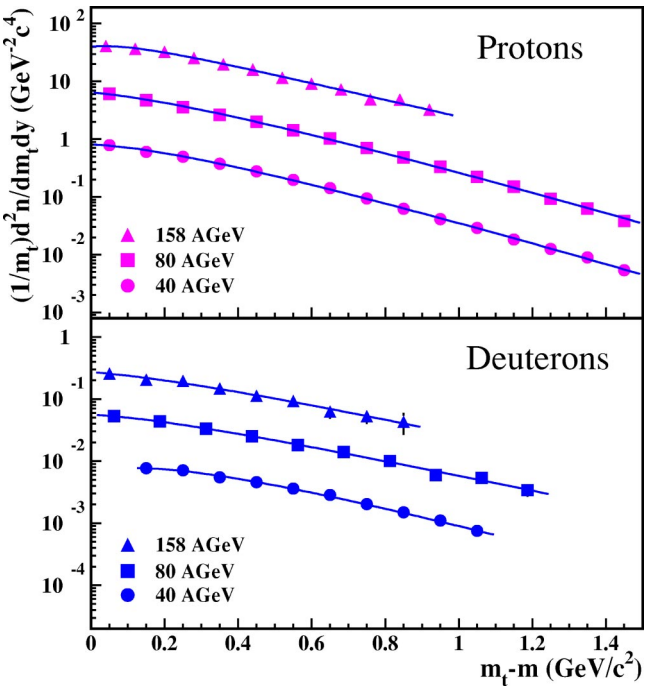

FIG. 3. (Color online) Transverse mass distributions for deuterons and protons near midrapidity in central Pb+Pb collisions at 40, 80, and 158 A GeV. The solid lines illustrate the two exponential fit of Eq. (2) to the data.

The above observations, an increase with mass of the inverse slope parameter, a deviation of the m_t spectra from an exponential shape at small transverse mass as well as the evolution of these features with centrality and beam energy are the predicted characteristics of radial collective expansion [20–22]. In agreement with the measurement these are

TABLE III. Particle yield dn/dy, inverse slope T, and mean transverse mass $\langle m_t\rangle - m$ for deuterons and protons in central Pb+Pb collisions at beam energies E_{beam} of 40, 80, and 158 A GeV. For completeness, the yields from 11.6 and 10.8 A GeV Au+Au collisions [14,34] are also shown. The errors are statistical.

Particle	E_{beam} (AGeV)	dn/dy	T (MeV)	$\langle m_t\rangle - m$ (MeV/c^2)
Deuteron	158	0.33±0.03	425±39	540±50
	80	0.59±0.04	360±15	467±20
	40	1.02±0.05	339±9	444±13
	11.6	5.00±0.50	-	395±35
Proton	158	29.6±0.9	308±9	413±13
	80	30.1±1.0	260±11	364±16
	40	41.3±1.1	257±11	367±16
	10.8	60.0±1.5	255±10	355±15

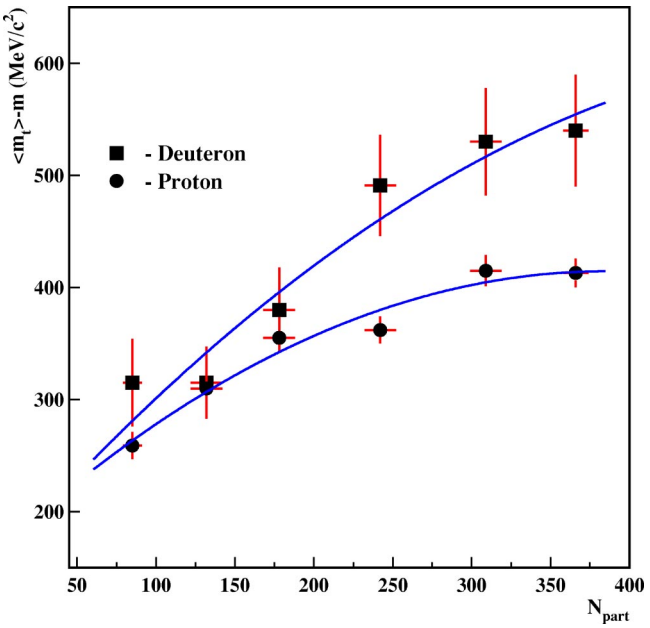

FIG. 4. (Color online) Average transverse mass $\langle m_t \rangle - m$ for deuterons ($2.0 < y < 2.5$) and for protons ($2.4 < y < 2.8$) as a function of N_{part} in 158*A* GeV Pb+Pb collisions. Overlaid are polynomial fits to underline the trend. The errors are statistical.

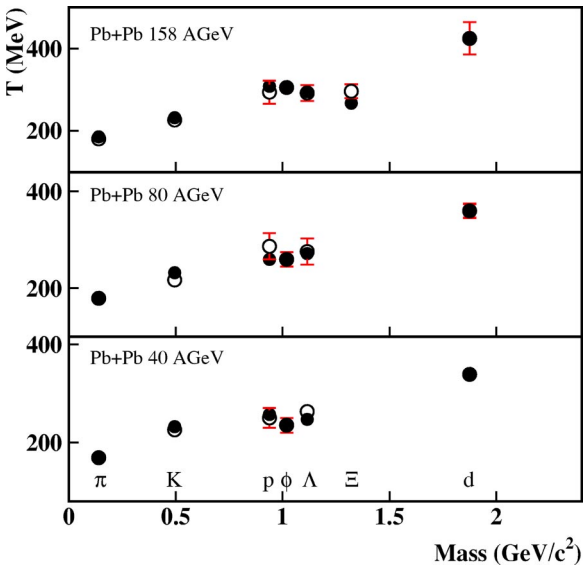

FIG. 5. (Color online) Inverse slope parameters T for a variety of particle species measured by NA49 near midrapidity in central Pb+Pb collisions at 40, 80, and 158 *A* GeV beam energies. Solid and open points are for particles and antiparticles, respectively. The data for π^- and $K^\pm$ are from Ref. [39], for Λ and Ξ baryons from Ref. [33] and Refs. [40,41], respectively, and for ϕ mesons from Ref. [42]. The data for Λ at 40, 80, and 158 *A* GeV, and for ϕ at 40 and 80 *A* GeV are preliminary. The results for p and d were obtained in this work. The quoted errors are statistical.

expected to be stronger in central than in peripheral collisions.

Transverse mass spectra at the top SPS energy have been studied by several experiments. It was realized that the inverse slope T of the transverse mass distribution increases steadily with the mass of the considered particle (for a review see Ref. [35]). This was explained as arising from the relativistic superposition of the local thermal distribution with the velocity field created by radial collective flow [22,36,37]. A possible deviation from this systematics observed for the multistrange baryons Ξ and Ω was discussed in Ref. [38].

The present data together with those recently obtained by NA49 [33,39–42] extend the results on mass systematics of the inverse slope parameter to the lower region of SPS energy and more species of emitted particles, from pions to deuterons. A compilation is shown in Fig. 5. The previous observation of an increase of the inverse slope parameter with increasing mass of emitted particles in central Pb+Pb collisions at 158*A* GeV is supported by the measurements at 40 and 80 *A* GeV beam energies. It is also seen from the figure that the inverse slopes for light particles (π^- and $K^\pm$) show no visible variation with beam energy (within errors) whereas for heavier species (p, d, Λ, and ϕ) the inverse slopes exhibit a systematic increase with increasing beam energy in the SPS energy range.

As mentioned above, the deuterons are assumed to be formed through the coalescence of protons and neutrons at the very latest stage of the reaction. Due to space-momentum correlation, most probably caused by radial collective flow, the slope parameter of deuterons is much higher than that of protons at all energies. Since deuterons are formed at freeze-out, they have not experienced directly the push of collective motion, but they contain the flow effect accumulated by their constituent nucleons. In order to explain the higher slope of deuterons as compared to protons quantitatively, one has to assume a uniform density distribution of the source with a sharp surface (boxlike profile) as was considered by Polleri *et al.* [23] and by Scheibl and Heinz [24], while a Gaussian shape was employed in the coalescence model of Llope *et al.* [43].

The deuteron measurement together with the measurement of protons allows the determination of the deuteron coalescence parameter B_2, which can be calculated from Eq. (1) for $A=2$. The resulting values of B_2 at small p_t measured in the rapidity bin $2.0 < y < 2.5$ are plotted versus the number of participating nucleons N_{part} in the top panel of Fig. 6. They are compared with data deduced from the NA52 experiment [17]. Good agreement is observed between both results. The numerical values of B_2 are tabulated in Table IV.

In the most central Pb+Pb interactions the coalescence parameter ($B_2 \simeq 4.5 \times 10^{-4}$ GeV$^2/c^3$) is nearly one-tenth of that measured for the most peripheral events, thus exhibiting a strong centrality dependence. This observation resembles the drastic drop of B_2 with increasing energy and may also imply a changing effective freeze-out volume of the emission source arising from the dynamics of the expansion.

The B_2 parameter can be related through the coalescence models to the size of the particle emission source [4–7]. The dynamics of the collisions is believed to be important for the coalescence mechanism. The model [24] explicitly considers rapid collective expansion of the collision zone in a density matrix approach for coalescence and finds the connection between the value of B_2 and the volume of homogeneity (the

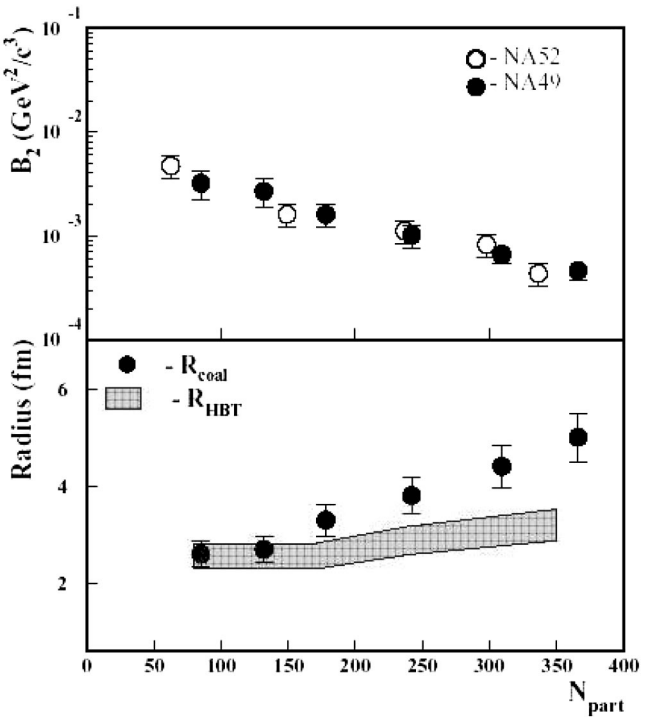

FIG. 6. (Color online) Top: Deuteron coalescence factor B_2 in the rapidity interval $2.0<y<2.5$ at 158*A* GeV Pb+Pb collisions near zero p_t plotted as a function of the number of participating nucleons N_{part} (full dots). The measurements are compared to the results of the NA52 experiment [17] at $y=3.7$ ($y=2.1$ reflected at midrapidity $y_{cm}=2.9$) (open dots). Bottom: Source radii R_{coal} extracted from the measured B_2 values in the context of the coalescence model [24] (full dots) and $R_{HBT}=(R_{side}^2 R_{long})^{1/3}$ calculated from the HBT data for correlations of $\pi\pi$ [44] (preliminary), *KK* [46,47], and *pp* [45] pairs (shaded band width indicating the estimated uncertainties). For details, see the text.

effective interaction volume) as $B_2 \propto 1/V_{hom}$ [see Eq. (6.3) of Ref. [24]]. From V_{hom} one can calculate a coalescence radius $R_{coal}=V_{hom}^{1/3}$ and compare it to the radius of homogeneity $R_{HBT}=(R_{side}^2 R_{long})^{1/3}$ obtained from Bose-Einstein correlations. Here R_{side} and R_{long} are the effective transverse and longitudinal dimensions of the emission region at freeze-out extracted from HBT interferometry.

Using the prescription of the model and the results of B_2 one can extract R_{coal} for each centrality bin. The result is displayed in the bottom panel of Fig. 6 by solid points. R_{HBT} derived from recent HBT results of NA49 is also depicted in the figure as a shaded band with a width representing the estimated uncertainty of the data.

TABLE IV. Coalescence parameter B_2 in 158*A* GeV Pb+Pb collisions at nearly zero p_t for six centrality bins specified by the mean numbers of participating nucleons $\langle N_{part}\rangle$. The estimated total errors are quoted.

$\langle N_{part}\rangle$	366	309	242
$B_2\times 10^4$ (GeV$^2/c^3$)	4.5±1.0	6.5±1.5	10.0±2.5
$\langle N_{part}\rangle$	178	132	85
$B_2\times 10^4$ (GeV$^2/c^3$)	16.0±4.0	27.0±8.0	32.0±9.0

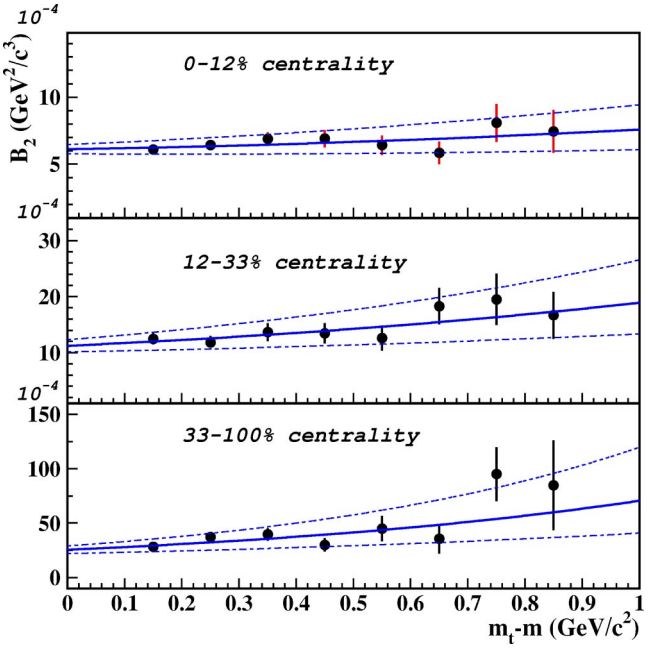

FIG. 7. (Color online) Coalescence factor B_2 for 158*A* GeV Pb+Pb reaction as a function of the deuteron transverse mass m_t-m for three centrality cuts. Curves show exponential fits of the form $B_2(m_t)=a\ \exp[c(m_t-m)]$. The dotted lines represent the effect of the $\pm 1\sigma$ errors of the fitted parameter c. The error bars are statistical.

It is important to note that the radius parameters used for comparison should be taken at similar m_t values in both the HBT and coalescence analysis, i.e., at m_t near the nucleon mass. For this calculation the dependence of HBT radii on N_{part} measured for pions at $m_t=0.2$ GeV/c^2 [44] was scaled to $m_t \simeq m_p$ using the m_t dependence of HBT radius parameters obtained from the correlation study of $\pi\pi$ [44], *pp* [45], and *KK* [46,47] pairs each of them measured at different m_t values in central 158*A* GeV Pb+Pb collisions.

It is observed that the effective source radius derived from B_2 rises more steeply with increasing N_{part} than that obtained from the HBT analysis. Towards central collisions an obvious discrepancy develops. Moreover, there is also a difference in the energy dependence of the coalescence and HBT radii. Namely, the difference in B_2 in central Pb+Pb collisions at 40 and 158 *A* GeV suggests about 30% difference in the coalescence radii for these energies, which is not seen in the HBT radii [44].

The dependence of the coalescence parameter B_2 on the deuteron transverse mass m_t-m is displayed in Fig. 7 for three centrality regions covering (0–12)%, (12–33)% and (33–100)% of σ_{tot}. The solid lines are exponential fits of the form $B_2(m_t)=a\ \exp[c(m_t-m)]$. The figure demonstrates that the coalescence probability B_2 increases at large m_t values in all three centrality selected data samples. This effect is connected to the difference in inverse slopes between deuterons and protons and can be explained as a consequence of the

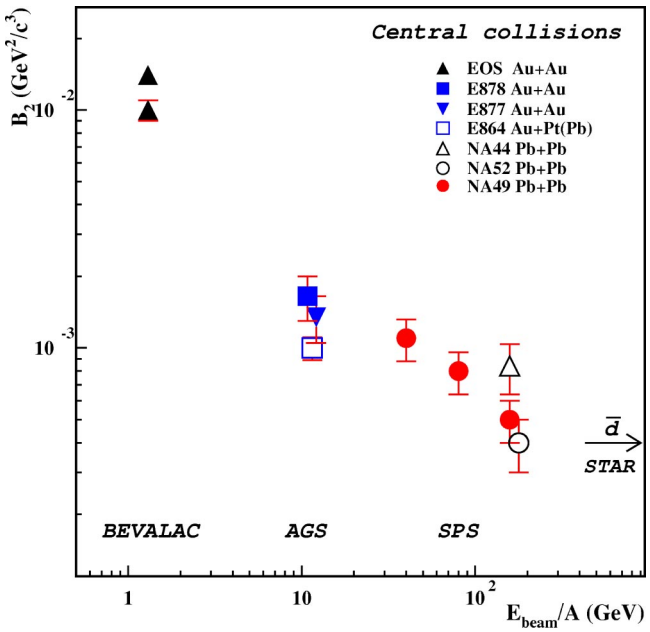

FIG. 8. (Color online) Coalescence factor B_2 for central Pb+Pb collisions at 40, 80, and 158 *A* GeV beam energies reviewed together with those from the Bevalac [10], AGS [12,13,16], and SPS [17,18]. Only data for midrapidity in central collisions of heavy systems are shown. The result for antideuterons from RHIC measured by STAR in Au+Au collisions [48] is also quoted.

interplay between transverse flow and the constant source density profile [23,24]. While the first two more central bins represent reasonably exclusive cuts on event geometry, the third more peripheral bin represents events averaged over a large range in collision geometry. However, it is believed that in very peripheral collisions there will be no m_t dependence of B_2 because the inverse slopes for deuteron and proton approach the same value (see Fig. 4). The AGS [14] and other SPS measurements [18,19] also reported that B_2 increases with m_t, thus exhibiting the same trend as the present results.

It should be noted that the proton and deuteron distributions used for B_2 calculations at 158 *A*GeV are measured not in exactly the same but partially overlapping rapidity intervals. This introduces some uncertainty which is estimated to be entirely contained within the quoted systematic errors for B_2. To give the numerical values, if the proton data at rapidity $2.4<y<2.8$ are corrected to the rapidity interval of the deuteron measurements $(2.0<y<2.5)$ the proton yield dn/dy increases by 5% and the inverse slope decreases by 10–15 MeV at most. This results in an $\approx$10% reduction of B_2 at small m_t values and a slightly steeper increase with m_t resulting in an about 10% increase at $m_t-m=1.0$ GeV/c^2. For above corrections the proton data from NA49 measured in a wide rapidity range [27,29] were used.

The B_2 values measured at 40, 80, and 158 *A*GeV beam energies for central Pb+Pb collisions are displayed in Fig. 8 and compared to measurements at other energies. The previously observed decrease of B_2 with beam energy is supported by the present measurements. The data show a continuous decrease of B_2 of at least a factor of 2 from AGS to the highest SPS energy.

V. SUMMARY

In central 158*A* GeV Pb+Pb collisions near midrapidity the mean transverse mass $\langle m_t\rangle-m$ for deuterons ($\simeq$540 MeV/c^2) is considerably larger than that for protons ($\simeq$415 MeV/c^2). Towards more peripheral collisions both decrease converging to $\langle m_t\rangle-m\simeq 200-250$ MeV/c^2. The spectra show a deviation from an exponential behavior at small m_t, which is more pronounced in central than in peripheral reactions. The deviation from the simple exponential form was also found for the deuteron and proton m_t spectra in central Pb+Pb reactions at 40 and 80 *A* GeV incident energies, and the mean transverse mass values are smaller than those in central 158*A* GeV collisions.

The coalescence parameter B_2 shows a trend to increase at large transverse mass m_t. The observed increase in B_2 with transverse mass as well as the larger inverse slope parameter T for deuterons than for protons support a model which assumes that the radial density profile of the emission source is close to a box shape and the transverse expansion velocity profile is nearly linear.

The coalescence factor in the most central bin is measured to be $B_2\simeq 4.5\times 10^{-4}$ GeV$^2/c^3$. It increases by about an order of magnitude when approaching the most peripheral collisions, thus exhibiting a strong dependence on the size of the collision zone. B_2 decreases steadily with beam energy within the SPS energy range.

The radius of the particle emission source derived from the B_2 measurement is in reasonable agreement with that from Bose-Einstein correlations in peripheral and mid-central Pb+Pb collisions. Approaching central collisions the former rises faster than the value obtained from the correlation analysis.

In summary, the observations are qualitatively consistent with the main features predicted by modern coalescence models that include the presence of a strong collective expansion in high energy nucleus-nucleus collisions of heavy nuclei.

ACKNOWLEDGMENTS

This work was supported by the Director, Office of Energy Research, Division of Nuclear Physics of the Office of High Energy and Nuclear Physics of the U.S. Department of Energy (DE-ACO3-76SFOOO98 and DE-FG02-91ER40609), the U.S. National Science Foundation, the Bundesministerium fur Bildung und Forschung, Germany, the Alexander von Humboldt Foundation, the Polish State Committee for Scientific Research (2 P03B 130 23, SPB/CERN/P-03/Dz 446/2002-2004, 2 P03B 02418, and 2 P03B 13023), the Hungarian Scientific Research Foundation (T032648, T14920 and T32293), Hungarian National Science Foundation, OTKA, Grant No. F034707, the EC Marie Curie Foundation, and the Polish-German Foundation.

[1] For review see *Proceedings of the Quark Matter 2002*, edited by H. Gutbrod, I. Aichelin, and K. Werner [Nucl. Phys. **A715**, 1c (2003)].
[2] T. Alber *et al.*, NA49 Collaboration, Phys. Rev. Lett. **75**, 3814 (1995).
[3] L. P. Csernai and J. I. Kapusta, Phys. Rep. **131**, 223 (1986).
[4] A. Mekjian, Phys. Rev. Lett. **38**, 640 (1977); S. Das Gupta and A. Z. Mekjian, Phys. Rep. **72**, 131 (1981).
[5] H. Sato and K. Yazaki, Phys. Lett. **98B**, 153 (1981).
[6] R. Bond *et al.*, Phys. Lett. **71B**, 43 (1977).
[7] S. Mrówczyński, Phys. Lett. B **277**, 43 (1992).
[8] S. T. Butler and C. A. Pearson, Phys. Rev. **129**, 836 (1963); A. Schwarzschild and Č. Zupančič, *ibid.* **129**, 854 (1963).
[9] H. H. Gutbrod *et al.*, Phys. Rev. Lett. **37**, 667 (1976); M.-C. Lemaire *et al.*, Phys. Lett. **85B**, 38 (1979); S. Nagamiya *et al.*, Phys. Rev. C **24**, 971 (1981); R. L. Auble *et al.*, *ibid.* **28**, 1552 (1983).
[10] S. Wang *et al.*, EOS Collaboration, Phys. Rev. Lett. **74**, 2646 (1995).
[11] J. W. Cronin *et al.*, Phys. Rev. D **11**, 3105 (1975); W. Bozzoli *et al.*, Nucl. Phys. **B144**, 317 (1978).
[12] J. Barrette *et al.*, E877 Collaboration, Phys. Rev. C **50**, 1077 (1994); T. Abbott *et al.*, E802 Collaboration, *ibid.* **50**, 1024 (1994); N. Saito *et al.*, E886 Collaboration, *ibid.* **49**, 3211 (1994).
[13] M. J. Bennett *et al.*, E878 Collaboration, Phys. Rev. C **58**, 1155 (1998).
[14] L. Ahle *et al.*, E802 Collaboration, Phys. Rev. C **60**, 064901 (1999).
[15] J. Barrette *et al.*, E877 Collaboration, Phys. Rev. C **61**, 044906 (2000).
[16] T. A. Armstrong *et al.*, E864 Collaboration, Phys. Rev. C **61**, 064908 (2000).
[17] G. Ambrosini *et al.*, NA52 Collaboration, New J. Phys. **1**, 221 (1999).
[18] A. G. Hansen *et al.*, NA44 Collaboration, Nucl. Phys. **A661**, 387C (1999); I. G. Bearden *et al.*, NA44 Collaboration, Eur. Phys. J. C **23**, 237 (2002).
[19] S. V. Afanasiev *et al.*, NA49 Collaboration, Phys. Lett. B **486**, 22 (2000).
[20] H. Sorge, J. L. Nagle, and B. S. Kumar, Phys. Lett. B **355**, 27 (1995); J. Sollfrank *et al.*, Z. Phys. C **52**, 593 (1991); U. Heinz, Nucl. Phys. **A610**, 264c (1996).
[21] U. Heinz *et al.*, Phys. Lett. B **382**, 181 (1996); S. Chapman, J. R. Nix, and U. Heinz, Phys. Rev. C **52**, 2694 (1995).
[22] P. Braun-Munzinger, J. Stachel, J. P. Wessels, and N. Xu, Phys. Lett. B **344**, 43 (1995); H. Appelshäuser *et al.*, NA49 Collaboration, Eur. Phys. J. C **2**, 661 (1998); E. Schnedermann, J. Sollfrank, and U. Heinz, Phys. Rev. C **48**, 2462 (1993).
[23] A. Polleri *et al.*, Phys. Lett. B **419**, 19 (1998); **473**, 193 (2000).
[24] R. Scheibl and U. Heinz, Phys. Rev. C **59**, 1585 (1999).
[25] J. L. Nagle *et al.*, Phys. Rev. C **53**, 367 (1996).
[26] S. V. Afanasiev *et al.*, NA49 Collaboration, Nucl. Instrum. Methods Phys. Res. A **430**, 210 (1999).
[27] G. E. Cooper, NA49 Collaboration, Nucl. Phys. **A661**, 362c (1999).
[28] F. Siklér *et al.*, NA49 Collaboration, Nucl. Phys. **A661**, 45c (1999).
[29] H. Appelshäuser *et al.*, NA49 Collaboration, Phys. Rev. Lett. **82**, 2471 (1999).
[30] K. Werner, Phys. Rep. **232**, 87 (1993).
[31] H. Sorge, Phys. Rev. C **52**, 3291 (1995).
[32] R. A. Fini *et al.*, WA97 Collaboration, J. Phys. G **27**, 375 (2001).
[33] A. Mischke *et al.*, NA49 Collaboration, Nucl. Phys. **A715**, 453C (2003).
[34] L. Ahle *et al.*, E802 Collaboration, Phys. Rev. C **57**, R466 (1998); B. B. Back *et al.*, E917 Collaboration, *ibid.* **66**, 054901 (2002).
[35] J. B. Kinson, J. Phys. G **25**, 143 (1999).
[36] G. Roland *et al.*, NA49 Collaboration, Nucl. Phys. **A638**, 91c (1998).
[37] I. G. Bearden *et al.*, NA44 Collaboration, Phys. Rev. Lett. **78**, 2080 (1997).
[38] H. van Hecke, H. Sorge, and N. Xu, Nucl. Phys. **A661**, 493c (1999).
[39] S. V. Afanasiev *et al.*, NA49 Collaboration, Phys. Rev. C **66**, 054902 (2002).
[40] S. V. Afanasiev *et al.*, NA49 Collaboration, Phys. Lett. B **538**, 275 (2002).
[41] H. Appelshäuser *et al.*, NA49 Collaboration, Phys. Lett. B **444**, 523 (1998).
[42] S. V. Afanasiev *et al.*, NA49 Collaboration, Phys. Lett. B **491**, 59 (2000); V. Friese *et al.*, NA49 Collaboration, nucl-ex/0305017.
[43] W. J. Llope *et al.*, Phys. Rev. C **52**, 2004 (1995); B. Monreal *et al.*, *ibid.* **60**, 031901 (1999).
[44] C. Blume *et al.*, NA49 Collaboration, Nucl. Phys. **A715**, 55c (2003).
[45] H. Appelshäuser *et al.*, NA49 Collaboration, Phys. Lett. B **467**, 21 (1999).
[46] S. V. Afanasiev *et al.*, NA49 Collaboration, Phys. Lett. B **557**, 157 (2003).
[47] I. G. Bearden *et al.*, NA44 Collaboration, Phys. Rev. Lett. **87**, 112301 (2001).
[48] C. Adler *et al.*, STAR Collaboration, Phys. Rev. Lett. **87**, 262301 (2001).